frontiers | Frontiers in Energy Research

TYPE Original Research
PUBLISHED 14 November 2023
DOI 10.3389/fenrg.2023.1256000

Check for updates

OPEN ACCESS

EDITED BY
Chi Lau,
Teesside University, United Kingdom

REVIEWED BY
Davide Papurello,
Polytechnic University of Turin, Italy
Houcheng Zhang,
Ningbo University, China
Wenjia Li,
Tianjin University, China

*CORRESPONDENCE
Liqiang Duan,
dlq@ncepu.edu.cn

RECEIVED 10 July 2023
ACCEPTED 19 October 2023
PUBLISHED 14 November 2023

CITATION
Bian J and Duan L (2023), Study on MCFC-integrated GSCC systems with SEGR in parallel or series and $CO_2$ capture.
*Front. Energy Res.* 11:1256000.
doi: 10.3389/fenrg.2023.1256000

COPYRIGHT
© 2023 Bian and Duan. This is an open-access article distributed under the terms of the Creative Commons Attribution License (CC BY). The use, distribution or reproduction in other forums is permitted, provided the original author(s) and the copyright owner(s) are credited and that the original publication in this journal is cited, in accordance with accepted academic practice. No use, distribution or reproduction is permitted which does not comply with these terms.

# Study on MCFC-integrated GSCC systems with SEGR in parallel or series and $CO_2$ capture

Jing Bian and Liqiang Duan*

Key Laboratory of Power Station Energy Transfer Conversion and System, School of Energy, Power and Mechanical Engineering, North China Electric Power University, Beijing, China

In this paper, two new molten carbonate fuel cell (MCFC)-integrated gas–steam combined cycle (GSCC) systems with selective exhaust gas recirculation (SEGR) and $CO_2$ capture are proposed and analyzed. The $CO_2$ concentration in the gas turbine emission is increased because $CO_2$ is selectively recycled with the help of SEGR. Molten carbonate fuel cells (MCFCs) are another way to increase $CO_2$ concentration in the gas turbine flue gas by translating only $CO_2$ from the cathode to the anode. In these two new gas–steam combined cycle systems, SEGR connected with MCFC, either in parallel or series, increases $CO_2$ concentration beyond 11%. A gas–steam combined cycle system combined with MCFC and $CO_2$ capture without SEGR is used as the reference system. Aspen Plus software is adopted to build the system models, and the performances of different systems are discussed and compared. The research results reveal that for the MCFC-integrated gas–steam combined cycle system with SEGR in series and $CO_2$ capture, the $CO_2$ concentration of gas turbine exhaust increases to 11.72% and the thermal efficiency is 56.29% when the overall $CO_2$ capture rate is 88.16%, which is 1.13% higher than that of the reference system; for the MCFC-integrated gas–steam combined cycle system with SEGR in parallel and $CO_2$ capture, the $CO_2$ concentration of gas turbine exhaust increases to 14.15% and the thermal efficiency is 56.62%, which is 1.46% higher than that of the reference system. Furthermore, the economic analysis results show that the economic performances of new systems are mainly influenced by MCFC cost and will be gradually improved with the decrease in the MCFC cost.

KEYWORDS

**gas turbine, molten carbonate fuel cell, selective exhaust gas recirculation, $CO_2$ emissions, economic analysis**

## 1 Introduction

The topic of $CO_2$ emission is attracting considerable attention with the rise in global warming, which poses a severe hazard to human health and survival. Total $CO_2$ discharge in China has increased from 9.122 billion tons (2011) to 9.912 billion tons (2020) (Miao et al., 2022). $CO_2$ emissions are mainly generated from fossil fuel-fired power systems, such as coal-fired power generation systems and gas–steam combined cycle (GSCC) systems. Although the gas–steam combined cycle has high efficiency, capturing $CO_2$ from the GSCC system is still a focus of attention in various countries since natural gas is usually applied as a fuel and still emits a large amount of $CO_2$. The F-class gas turbine (GT) is widely applied (Tsukagoshi et al., 2007), and its turbine inlet temperature can reach up to 1,400°C (ElKady et al., 2009). Choi et al. (2014) found that

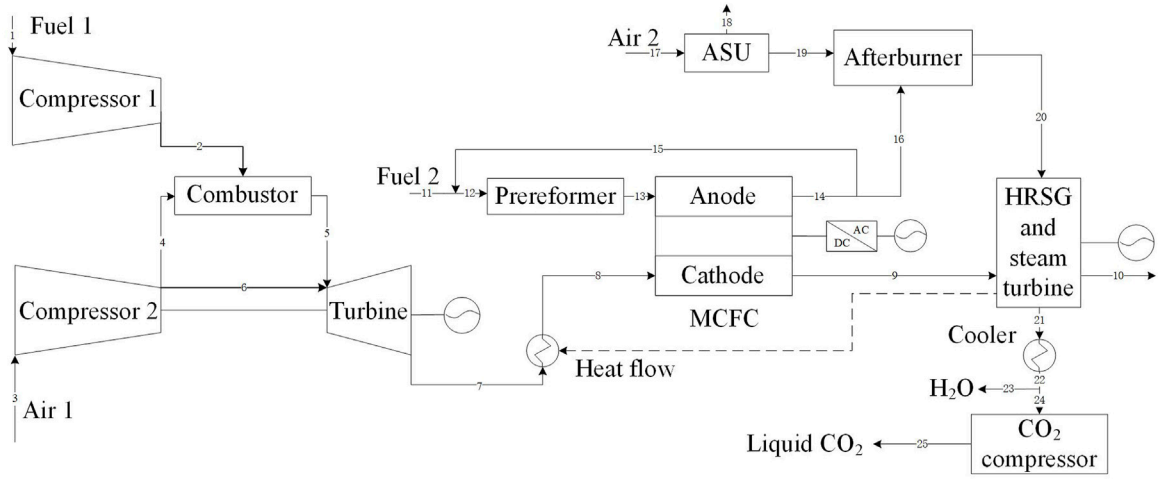


FIGURE 1
Flowchart of the GSCC system combined with MCFC and $CO_2$ capture without flue gas recirculation.

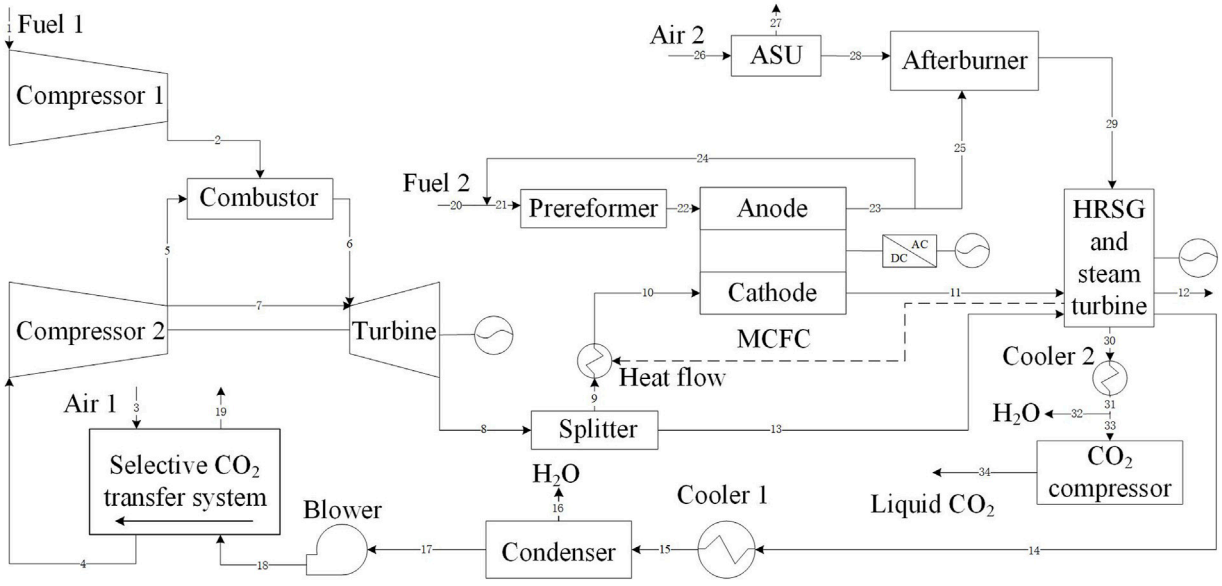


FIGURE 2
Flowchart of the MCFC-integrated GSCC system with SEGR in parallel and $CO_2$ capture.

using the F-class GT, for the GSCC system integrated with a solid oxide fuel cell (SOFC), without carbon capture, the efficiency reaches almost 70%.

Conventional $CO_2$ capture methods usually result in a significant decrease in efficiency and output power. Compared with the conventional $CO_2$ capture techniques, MCFC has special advantages of increasing the efficiency of the entire system. $CO_2$ and $O_2$ from the GT exhaust gas can form carbonate ions in the cathode of MCFC, which are carried to the anode by the molten electrolyte of MCFC. After the carbonate ions react with fuels such as $CH_4$ or $H_2$, $H_2O$ and $CO_2$ are generated at the anode; therefore, after the combustion of anode flue gas and pure $O_2$ in the afterburner, only $CO_2$ and $H_2O$ are left. The MCFC has higher efficiency and lower cost than the phosphoric acid fuel cell (PAFC) and a more simple structure than the SOFC (Zhao and Hou, 2022). Carapellucci et al. (2019) compared the systems of the steam power plant (SPP) combined with MCFC and the SPP combined with the monoethanolamine (MEA) method. The results showed that the system of SPP combined with MCFC had a higher overall efficiency and $CO_2$ removal capacity.

Selective exhaust gas recirculation (SEGR) is a type of technique to recycle $CO_2$ from GT flue gas with membranes

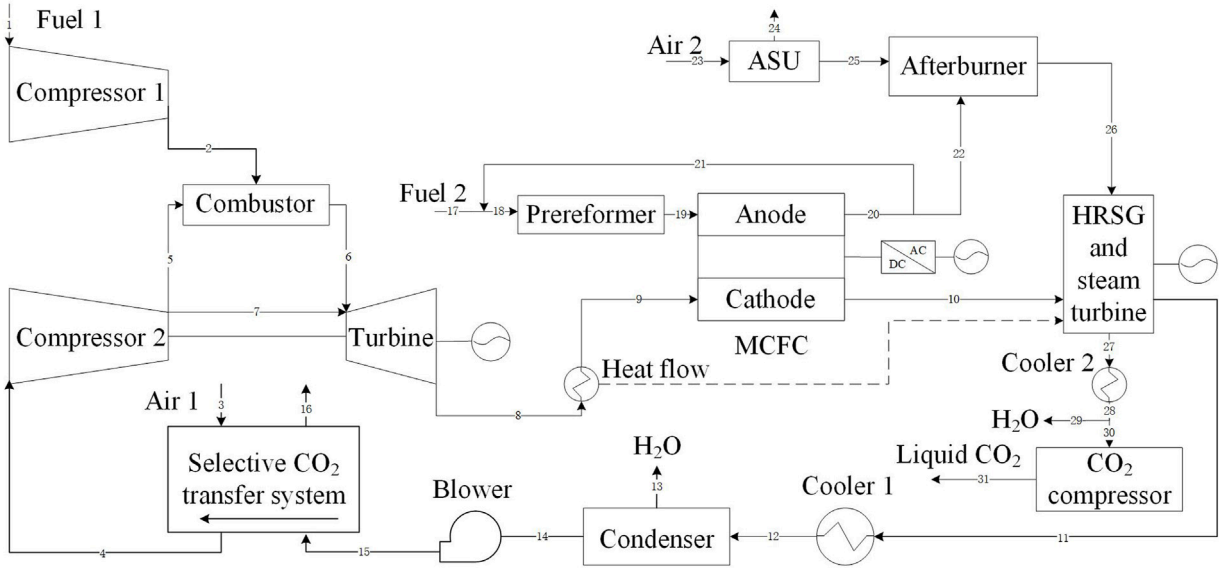


FIGURE 3
Flowchart of the MCFC-integrated GSCC system with SEGR in series and $CO_2$ capture.

to increase the $CO_2$ concentration ($c_{CO_2}$) in the cycle. $CO_2$ is selectively conveyed through membranes from the exhaust gas; therefore, higher $c_{CO_2}$ is possible in the emission. As $N_2$ and $H_2O$ in the exhaust gas are ideally not recirculated, the flow rate of emitted gas is reduced. When the air is applied as the sweep gas, SEGR can be driven by the $c_{CO_2}$ difference between the air side and the flue gas side, which means that the $CO_2$ can be enriched by SEGR with nearly no energy consumption and without requiring pressurization equipment. Bellas et al. (2019) conducted experiments on a micro-GT with SEGR and revealed that $c_{CO_2}$ in the exhaust gas was significantly improved with the help of SEGR, and the nitrogen oxide (NOx) emissions were reduced. The $c_{CO_2}$ in the GT exhaust could be raised to 18% when SEGR and MEA were integrated into natural gas combined cycle (NGCC) plants (Herraiz et al., 2018). Diego et al. (2018) proved that SEGR effectively reduced the energy demand of the NGCC plant combined with MEA. Merkel et al. (2012) used the $H_2$-selective and $CO_2$-selective membranes to capture $CO_2$ formed in the integrated gasification combined cycle (IGCC) power plants. The research results revealed that there was a decrease in both capital cost and energy utilization compared with the cold absorption method of $CO_2$ capture.

Even though both the methods of MCFC and SEGR can enrich $CO_2$ with less energy consumption compared with the conventional $CO_2$ capture methods, there are still limitations to using either MCFC or SEGR alone. When MCFC is adopted alone, Milewski et al. (2013) verified with experiments that the performance of MCFC was deeply limited by the $c_{CO_2}$ of the cathode. When SEGR was adopted alone, Richard et al. (2017) studied that the rise in $c_{CO_2}$ of exhaust gas was limited, which could be 15–20 vol%. Therefore, if SEGR is integrated into MCFC, the $c_{CO_2}$ of exhaust gas can be additionally increased, and the performance of MCFC can be significantly improved, which has not been studied yet.

To reduce $CO_2$ emission with less energy consumption and increase the whole system performance, two GSCC systems combined with MCFC, SEGR, and $CO_2$ capture are proposed in this work. The SEGR operating in parallel with the GSCC system combined with MCFC is investigated in the first system; in the second system, the SEGR operating in series with the GSCC system integrated into MCFC is investigated. The thermal and economic performances of different systems are discussed and compared. The effects of the SEGR ratio and the $CO_2$ capture rate on the thermal efficiency and economic performance of new systems are examined.

## 2 Description of different systems

### 2.1 GSCC system integrated into MCFC and $CO_2$ capture (reference system)

In this study, the GSCC system combined with MCFC and $CO_2$ capture without SEGR is selected as the reference system, and the system flowchart is shown in Figure 1. After passing through compressor 1, the fuel (2) is supplied to the combustor. After passing through compressor 2, the air (3) is separated into compressed air (4) and (6). Compressed air (4) is supplied into the combustor; compressed air (6) is transferred into the GT as the coolant gas. The combustion chamber emission expands in the gas turbine to produce electricity, and the gas turbine flue gas is then transferred to the MCFC cathode. A portion of the anode flue gas (15) is sent to the pre-reformer to convert the fuel into $H_2$ and CO in order to prevent the carbon deposition problem (Duan et al., 2014). After being transported from the cathode, the

**TABLE 1 System simulation parameters.**

| | | |
|---|---|---|
| Ambient condition (Duan et al., 2014) | | 298.15 K, 1.01 atm |
| Generator efficiency (Duan et al., 2014) | | 99% |
| Compositions of air (Duan et al., 2014) | | $N_2$ 79% and $O_2$ 21% |
| *Gas turbine* | | |
| Mass flow of GT fuel (kg/s) | | 15 |
| Content of fuel | | $CH_4$ 100% |
| Lower heating value of fuel (kJ/kg) (Duan et al., 2014) | | 50,030 |
| Pressure ratio | | 16 |
| Turbine entrance temperature (K) | | 1,673 |
| *Membranes* | | |
| $CO_2/N_2$ selectivity (–) (Ramasubramanian et al., 2012) | | 140 |
| $CO_2$ permeance (gpu) (Ramasubramanian et al., 2012) | | 3,000 |
| *HRSG* | | |
| LP/MP/HP pressure (MPa) (Duan et al., 2014) | | 0.39/3.6/17.6 |
| Isentropic efficiency of LP/MP/HP (Duan et al., 2014) | | 92%/91%/90% |
| Mechanical efficiency of turbine (Duan et al., 2014) | | 99% |
| *Air separation unit* | | |
| Operating pressure (MPa) (Duan et al., 2015) | | 0.6 |
| Isentropic efficiency (Duan et al., 2015) | | 80% |
| *$CO_2$ compression* | | |
| Compression stage quantity (Duan et al., 2014) | | 3 |
| Exit pressure (atm) (Duan et al., 2014) | | 80 |
| Exit temperature (K) (Duan et al., 2014) | | 303.15 |
| *MCFC* | | |
| Mass flow of fuel (kg/s) | | 3.75 |
| Content of fuel | | $CH_4$ 100% |
| Lower heating value of fuel (kJ/kg) | | 50,030 |
| Area ($m^2$) | | 102,245 |
| Ratio of steam to carbon (Duan et al., 2014) | | 3.5 |
| Current density ($A/m^2$) (Duan et al., 2014) | | 1,500 |
| Fuel utilization rate | | 0.85 |
| Working temperature (K) (Duan et al., 2015) | | 923.15 |
| $\eta_{DC-AC}$ | | 95% |
| Active surface area ($m^2/m^3$) (Bian et al., 2020) | Anode | 2.7E5 |
| | Cathode | 3.0E5 |
| Thickness (mm) (Bian et al., 2020) | Anode | 0.6 |
| | Cathode | 0.6 |
| | Electrolyte | 1 |
| Electrical conductivity (S/m) (Bian et al., 2020) | Anode | 100 |
| | Cathode | 100 |
| | Electrolyte | 138.6 |

(Continued on following page)

**TABLE 1 (*Continued*) System simulation parameters.**

| | | |
|---|---|---|
| Standard exchange current (A/m²) (Bian et al., 2020) | Anode | 50 |
| | Cathode | 2 |
| Effective diffusivity (m²/s) (Bian et al., 2020) | Anode | 3.97E-6 |
| | Cathode | 1.89E-6 |

carbonate ions react with $H_2$ in the anode and produce $H_2O$ and $CO_2$ (Milewski et al., 2013). The cathode flue gas (9) has low $c_{CO_2}$ and high temperature after the electrochemical reaction, and after discharging heat in the heat recovery steam generator (HRSG), the cathode flue gas (9) is released into the atmosphere (10). In the afterburner, pure $O_2$ (19) generated from the air separation unit is utilized to combust the rest anode flue gas (16). Then, the afterburner flue gas (20) is supplied into the HRSG to release heat. Finally, the afterburner flue gas (21), consisting of $H_2O$ and $CO_2$, is condensed and compressed to generate the liquid $CO_2$ (25).

## 2.2 MCFC-integrated GSCC system with SEGR in parallel and $CO_2$ capture

The simplified flowchart of the MCFC-integrated GSCC system with SEGR in parallel and $CO_2$ capture is shown in Figure 2. The GT exhaust gas (8) is separated into two parts: (9) and (13). After being heated by the afterburner flue gas to 923.15 K (Duan et al., 2014), the flue gas (9) is transferred to the MCFC cathode. After being cooled in the HRSG and further cooled in cooler 1 to 353.15 K, exhaust gas (13) is supplied into the condenser to remove $H_2O$ (15). Then, the water-excluded flue gas (17) is blown into the selective $CO_2$ transfer system. The air mixed with $CO_2$ selected by the membranes is then compressed in compressor 2.

## 2.3 MCFC-integrated GSCC system with SEGR in series and $CO_2$ capture

Figure 3 shows a simplified flowchart of the MCFC-integrated GSCC system with SEGR in series and $CO_2$ capture. The GT flue gas (11) is cooled in HRSG and further cooled in cooler 1 to a temperature of 303.15 K. Then, the water-excluded flue gas (14) is blown into the selective $CO_2$ transfer system. The sweep air 1 (3) is transferred to the selective $CO_2$ transfer system.

# 3 System modeling

Aspen Plus software is adopted to establish the simulation models. In brief, the MCFC is simulated using a Fortran code, and the selective $CO_2$ transfer system is modeled using Aspen Custom Modeler. The new system parameters are obtained as shown in Table 1. During the establishment of the models, the suppositions to be considered are as follows (Bian et al., 2022):

1) Thermally insulated MCFC, and no entropy flow to the outside environment.
2) Constant membrane permeability, and the coupling impact is ignored.
3) Kinetic or potential energy effects are ignored.
4) Incompressible ideal gas and steady-state conditions are supposed.

The main equations of the MCFC model used in the Fortran code are listed in Table 2 (Eqs 1–25). To guarantee that the afterburner combustion gas contains only $CO_2$ and $H_2O$, the MCFC anode is supplied with pure $CH_4$. In Eq. 5, $\Delta G$ is the Gibbs free energy (kJ/kg) and $p_i$ represents the partial pressure of species i (MPa). In Eqs 8–11, j is the current density (A/m²); $j_0$ represents the exchange current density (A/m²); and $j_0^0$ is the standard exchange current density (A/m²). In Eq. 13, $R_{ohm}$ stands for the Ohmic polarization cell resistance ($\Omega \cdot m^2$); $\tau$ is the thickness (mm); and $\sigma$ is the electrical conductivity ($S/m^{-1}$). The gas transport models in porous media are used (Eqs 17–21) to calculate the gas partial pressures at the three-phase boundaries ($p_{i,TPB}$). $p_{i,TPB}$ represents the partial pressure of the species i at the three-phase boundary (MPa) and $D_{eff}$ is the effective diffusivity (m²/s).

The gas permeance equations are listed in Table 2 (Eq. 26). The selective $CO_2$ transfer system is arranged as counter-current. $Q_i$ is the permeability of the species i (kmol/(m²s · MPa)); $d\dot{n}_i$ represents the gas permeance of species i for a segment of area (kmol/s); A represents the area (m²); $p_{i,f}$ represents the partial pressure of the species i at the feed side (MPa); and $p_{i,p}$ represents the partial pressure of species i at the permeate side (MPa).

# 4 Model validation with experimentation

## 4.1 Gas turbine system model validation with literature data

The GT system model is validated with the data from Choi et al. (2014). In the literature, an F-class GSCC system with SOFC is studied. The specifications of the two GSCC systems are shown in Table 3. The simulated data are in excellent agreement with the literature data.

## 4.2 MCFC model validation using experiments

The model accuracy is validated using unit MCFC cell equipment, as shown in Figure 4A. The unit fuel cell includes

**TABLE 2 Main reaction equations.**

| *MCFC* | |
|---|---|
| Reforming reaction (Duan et al., 2014) | $CH_4 + H_2O \rightarrow CO + 3H_2$ (1) |
| | $CO + H_2O \rightarrow CO_2 + H_2$ (2) |
| Cathode reaction (Duan et al., 2014) | $0.5O_2 + CO_2 + 2e^- \rightarrow CO_3^{2-}$ (3) |
| Anode reaction (Duan et al., 2014) | $H_2 + CO_3^{2-} \rightarrow H_2O + CO_2 + 2e^-$ (4) |
| Ideal reversible voltage (Bian et al., 2020) | $E_{Nerst} = \frac{\Delta G}{nF} + \frac{RT}{nF}\ln[\frac{p_{H_2}(p_{O_2})^{0.5}p_{CO_2,ca}}{p_{H_2O}p_{CO_2,an}}]$ (5) |
| | $\Delta G = 242,000 - 45.8T$ (6) |
| Activation loss (Bian et al., 2020) | $\eta_{act} = \eta_{act,an} + \eta_{act,ca}$ (7) |
| | $\eta_{act,an} = \frac{RT}{\alpha nF}\ln\frac{jp_{H_2}}{j_{0,an}p_{H_2,TPB}}$ (8) |
| | $\eta_{act,ca} = \frac{RT}{\alpha nF}\ln\frac{j(p_{O_2})^{0.5}p_{CO_2,ca}}{j_{0,ca}(p_{O_2,TPB})^{0.5}p_{CO_2,ca,TPB}}$ (9) |
| | $j_{0,an} = j^0_{0,an}(p_{H_2})^{0.25}(p_{H_2O})^{0.25}(p_{CO_2,an})^{0.25}$ (10) |
| | $j_{0,ca} = j^0_{0,ca}(p_{O_2})^{0.375}(p_{CO_2,ca})^{-1.25}$ (11) |
| Ohmic loss (Arpornwichanop et al., 2013) | $\eta_{ohm} = jR_{ohm}$ (12) |
| | $R_{ohm} = \frac{\tau_{an}}{\sigma_{an}} + \frac{\tau_{elec}}{\sigma_{elec}} + \frac{\tau_{ca}}{\sigma_{ca}}$ (13) |
| Concentration loss (Arpornwichanop et al., 2013) | $\eta_{conc} = \eta_{conc,an} + \eta_{conc,ca}$ (14) |
| | $\eta_{conc,an} = \frac{RT}{2F}\ln(\frac{p_{H_2}p_{H_2O,TPB}p_{CO_2,an,TPB}}{p_{H_2,TPB}p_{H_2O}p_{CO_2,an}})$ (15) |
| | $\eta_{conc,ca} = \frac{RT}{2F}\ln(\frac{p_{CO_2,ca}(p_{O_2})^{0.5}}{p_{CO_2,ca,TPB}(p_{O_2,TPB})^{0.5}})$ (16) |
| | $p_{H_2,TPB} = p_{H_2} - \frac{RT\tau_{an}}{2FD_{eff,an}}j$ (17) |
| | $p_{H_2O,TPB} = p_{H_2O} + \frac{RT\tau_{an}}{2FD_{eff,an}}j$ (18) |
| | $p_{CO_2,an,TPB} = p_{CO_2,an} + \frac{RT\tau_{an}}{2FD_{eff,an}}j$ (19) |
| | $p_{O_2,TPB} = p_{O_2} - \frac{RT\tau_{ca}}{4FD_{eff,ca}}j$ (20) |
| | $p_{CO_2,ca,TPB} = p_{CO_2,ca} - \frac{RT\tau_{ca}}{2FD_{eff,ca}}j$ (21) |
| Actual MCFC voltage (Bian et al., 2022) | $V_{cell} = E_{Nerst} - \eta_{act} - \eta_{ohm} - \eta_{conc}$ (22) |
| MCFC power output (Bian et al., 2020) | $W_{MCFC} = A_c j V_{cell}$ (23) |
| Net power output | $W_{MCFC,net} = \eta_{DC-AC}W_{MCFC}$ (24) |
| MCFC thermal efficiency | $\eta_{MCFC} = \frac{W_{MCFC,net}}{m_{MCFC}LHV}$ (25) |
| *Selective $CO_2$ transfer system* | |
| Species i gas permeance (Franz et al., 2013) | $d\dot{n}_i = dA \cdot Q_i(p_{i,f} - p_{i,p})$ (26) |
| *Performance indicators* | |
| MCFC fuel utilization rate (Duan et al., 2015) | $U_{fuel} = 1 - \frac{m_{fuel,outlet}}{m_{fuel,inlet}}$ (27) |
| MCFC $CO_2$ utilization rate (Duan et al., 2015) | $U_{CO_2} = 1 - \frac{m_{CO_2,outlet}}{m_{CO_2,inlet}}$ (28) |
| Overall $CO_2$ capture rate (Duan et al., 2015) | $OCCR = \frac{m_{CO_2,capture}}{m_{CO_2,emissions}}$ (29) |

(Continued in next column)

**TABLE 2 (*Continued*) Main reaction equations.**

| *MCFC* | |
|---|---|
| Thermal efficiency of MCFC | $\eta_{MCFC} = \frac{W_{MCFC}}{m_{MCFC}LHV}$ (30) |
| Overall thermal efficiency | $\eta = \frac{W_{total,net}}{m_{MCFC}LHV + m_{GT}LHV}$ (31) |

a porous anode of Ni/Cr alloy, a porous cathode of NiO, and an electrolyte matrix filled with the combination of 62% $Li_2CO_3$ and 38% $K_2CO_3$. The experimental device consists of a temperature control facility, a gas flow control facility, and the unit fuel cell. The operating temperature is 650°C under atmospheric conditions. The electrochemical workstation is applied to set and measure the current density and voltage. The simulation and actual voltage values at different $c_{CO_2}$ are shown in Figure 4B. In this paper, the value of the error indicator RMSE is 0.014 V, which is calculated using Eq. 32. It is noticeable that the simulation results are in good agreement with the test values.

$$RMSE(x) = \sqrt{\frac{1}{N}\sum_{i=1}^{N}\left(I_i^{experimental} - I_i^{estimated}\right)^2}. \quad (32)$$

# 5 Results and discussion

In this section, results of the models with SEGR in parallel and series are discussed and compared with the reference system.

## 5.1 MCFC-integrated GSCC system with SEGR in parallel and $CO_2$ capture

The flowchart of an MCFC-integrated GSCC system with SEGR in parallel and $CO_2$ capture is shown in Figure 2. One part of the exhaust gas regenerated by the HRSG is supplied to the selective $CO_2$ transfer system. $CO_2$ is passed through membranes selectively and then supplied to the compressor with the sweep air.

Figure 5A shows the variations in the MCFC $CO_2$ utilization rate that is demanded to capture 88.16% of $CO_2$ produced by the combustion as a function of the SEGR for different selective $CO_2$ transfer rates (SCTRs). For a constant SCTR, the MCFC $CO_2$ utilization rate rises at a higher recirculation rate. This is because the $CO_2$ discharged by the selective $CO_2$ transfer system increases with the increase in the recirculation rate since the $c_{CO_2}$ in the exhaust gas is higher. A considerable amount of $CO_2$ is captured in the MCFC.

When the SCTR is held constant at 0.95 and the selective exhaust gas recirculation rate is increased from 0 to 0.7, the mass flow rate of sweep air decreases. The reason is that the turbine entrance temperature should be kept invariable. Therefore, the $c_{CO_2}$ in GT flue gas increases, and the $O_2$ concentration ($c_{O_2}$) decreases, as illustrated in Figure 5B. $O_2$ in the combustor exceeds the limit of 17% for F-class GT (Evulet et al., 2009), as shown in Figure 5B.

When the SCTR is held constant at 0.95 and the selective exhaust gas recirculation rate is raised from 0 to 0.7, the $c_{CO_2}$ is

**TABLE 3 GSCC specifications.**

| Parameter | Reference (Choi et al., 2014) | Simulation result |
|---|---|---|
| Turbine entrance temperature (K) | 1,673 | 1,673 |
| Turbine rotor entrance temperature (K) | 1,600 | 1,600 |
| Compressor pressure ratio | 16 | 16 |
| Turbine coolant rate to compressor intake (%) | 16 | 16 |
| Fuel mass flow of GT (kg/s) | 10.16 | 15 |
| Specific GT power (MJ/kg) | 18.07 | 19.28 |
| Specific ST power (MJ/kg) | 10.09 | 8.96 |
| Combined cycle power/fuel mass flow (MJ/kg) | 28.16 | 28.23 |
| Combined cycle efficiency (%) | 57.1 | 56.4 |

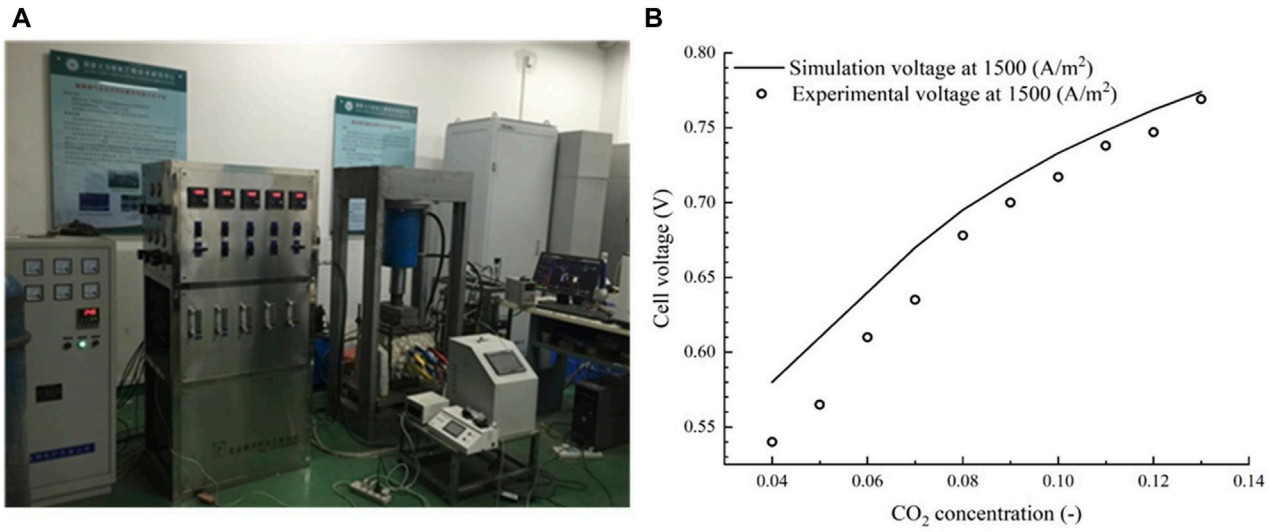


FIGURE 4
**(A)** Unit MCFC cell facility and **(B)** simulation and test voltages under various $c_{CO_2}$.

significantly influenced by the change in the SEGR. According to Eq. 5, the ideal reversible voltage mainly increases with the increase in $c_{CO_2}$ in GT exhaust gas. According to Eq. 16, the cathode concentration loss is reduced with the increase in $c_{CO_2}$. Therefore, the actual cell voltage increases with the increase in SEGR as the $c_{CO_2}$ increases, according to Eq. 22. As shown in Figure 5C, when the SEGR increases from 0.6 to 0.7, the slope of the voltage is smaller because of the significant decrease in the $O_2$ concentration, leading to a massive rise in the cathode concentration loss according to Eq. 16. When the SEGR is changed and the SCTR is held constant, the system thermal efficiency is principally affected by the output of MCFC. The output of MCFC is regulated by the voltage as the current density is maintained at 1500 A/m$^2$. As the SEGR is increased from 0 to 0.6, the system thermal efficiency increases as the voltage increases. With the increase in the SEGR, the sweep air mass flow rate decreases to maintain the invariable turbine entrance temperature, which gives rise to the reduction in the mass flow rate of the expanding gas into the gas turbine. Therefore, the output of GT is reduced with the increase in the SEGR. While the SEGR increases from 0.6 to 0.7, as the drop in the GT output is larger than the increase in the MCFC output, the system thermal efficiency decreases, as shown in Figure 5C.

## 5.2 MCFC-integrated GSCC system with SEGR in series and $CO_2$ capture

The flowchart of the MCFC-integrated GSCC system with SEGR in series and $CO_2$ capture is illustrated in Figure 3. After $CO_2$ is excluded by MCFC, the emission of GT is supplied to the selective $CO_2$ transfer system.

Figure 6A shows the changes in the MCFC $CO_2$ utilization rate required to capture 88.16% of $CO_2$ as a function of SCTRs. The more the $CO_2$ conveyed to the combustion air, the less the $CO_2$ utilization rate demanded by the MCFC.

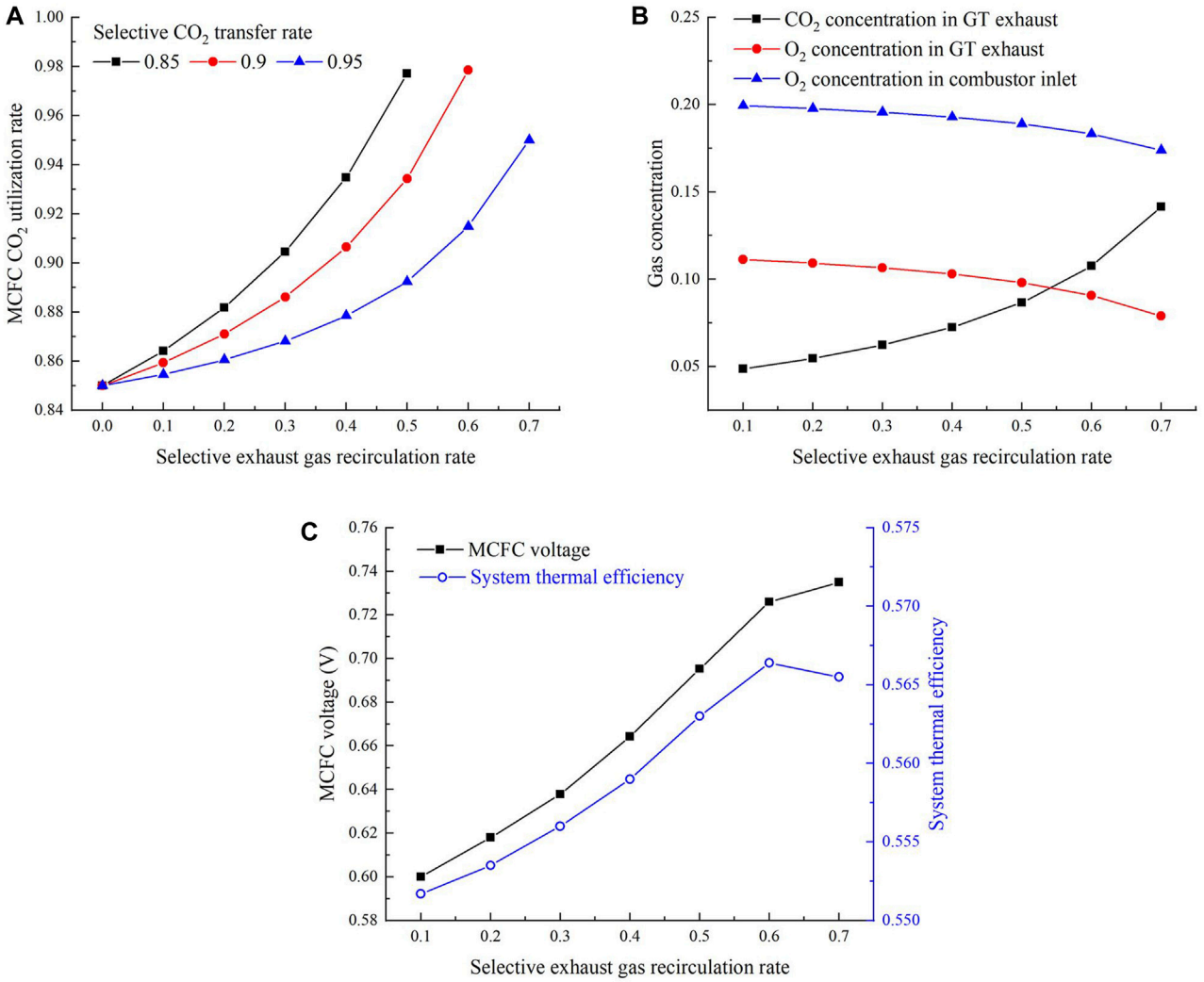


FIGURE 5
Impact of the SEGR on **(A)** $U_{CO_2}$, **(B)** gas concentration, and **(C)** MCFC voltage and system thermal efficiency (the OCCR is 88.16%).

When the SCTR increases from 0.65 to 0.91, the mass flow of sweep air (air 1) decreases to maintain the turbine entrance temperature constant; therefore, the $c_{CO_2}$ in GT exhaust increases, and the $c_{O_2}$ decreases, as illustrated in Figure 6B. As $O_2$ in the combustor must be maintained above 17 vol% for an F-class gas turbine, the largest $c_{CO_2}$ in GT exhaust gas can be achieved at 11.72% when the SCTR is 0.91.

When the SCTR increases from 0.65 to 0.91, the MCFC voltage is mainly regulated by the $c_{CO_2}$ in the GT exhaust gas as the $c_{CO_2}$ is influenced by the change in the SCTR. The MCFC voltage increases with the increase in the SCTR as the $c_{CO_2}$ increases, according to Eqs 5 and 16. When the SCTR increases from 0.9 to 0.91, the slope of the MCFC voltage is smaller because of the decrease in the $O_2$ concentration, as shown in Figure 6C. As the SCTR is varied, according to Eq. 23, the MCFC power output increases as the MCFC voltage increases and the current density is held constant. The system thermal efficiency increases as the MCFC power output increases, according to Eq. 25. However, with the increase in the SCTR, the sweep air mass flow rate decreases to maintain the invariable turbine entrance temperature, which gives rise to the reduction in the mass flow rate of the expanding gas into the gas turbine. Therefore, the output power of the GT is reduced with the increase in the SCTR. When the SCTR increases from 0.9 to 0.91, as the drop in the GT output is larger than the increase in the MCFC output, the system thermal efficiency decreases, as shown in Figure 6C.

## 5.3 Comparison of the results for different systems

The major operating parameters of the MCFC voltage and GSCC system for SEGR in series and parallel with MCFC are shown in Table 4. Parallel 96/90 denotes that the new system with SEGR in parallel operates with a 0.96 $CO_2$ utilization rate of MCFC and 0.9 SCTR of the membrane. Series 91/28, 90/36, and 85/46 denote that the new system with SEGR in series operates

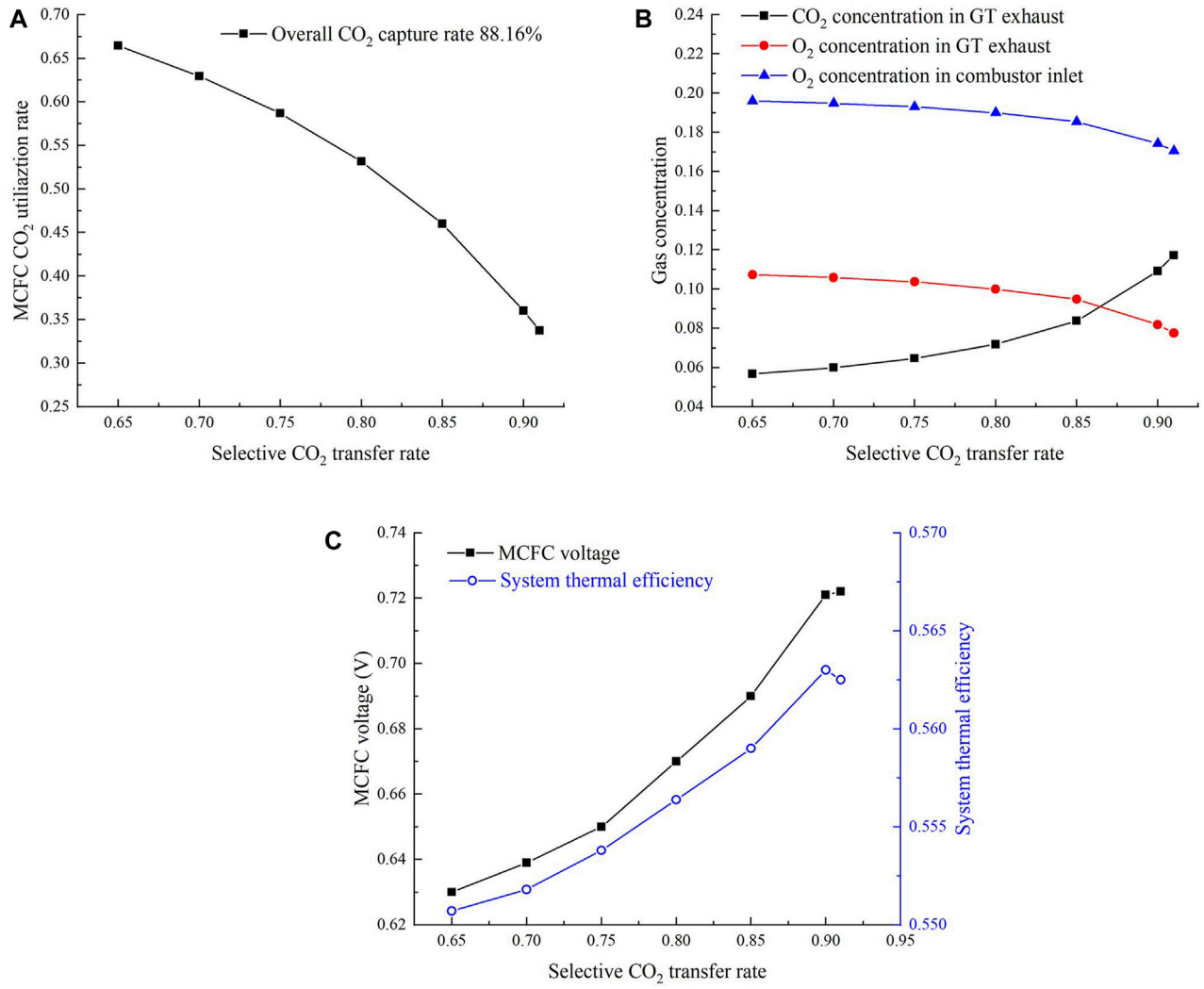


FIGURE 6
Impact of SCTR on **(A)** $U_{CO_2}$, **(B)** gas concentration, and **(C)** MCFC voltage and system thermal efficiency (SEGR in series when the OCCR is 88.16%).

with MCFC $CO_2$ utilization rates of 0.91, 0.9, and 0.85 and membrane SCTRs of 0.28, 0.36, and 0.46, respectively. An MCFC-integrated GSCC system with $CO_2$ capture and without SEGR is considered the reference system. The current density and the area of MCFC are held constant. The key stream data of different systems are shown in Table 4. The data on the streams from parallel 96/90 and series 90/36 are shown in detail in the Supplementary Material. The power and thermal efficiency of different systems are listed in Table 4. Compared with the reference system, there is an increase in the entire thermal efficiencies of the systems with SEGR in parallel and series. The efficiency of the parallel 96/90 system is greater than that of the series 90/36 system.

Figure 7A indicates the air mole flow rate at the compressor entrance and the GT net output. In contrast to the reference system, with the increase in the selective flue gas recirculation, to keep the GT inlet temperature constant at 1400°C, the air into the selective $CO_2$ transfer system decreases. Therefore, the air mole flow rate at the compressor inlet decreases, which results in the decrease in the GT output power, which is in contrast to the reference case. When the SCTR of the GSCC system with SEGR in series is reduced from 0.91 to 0.85, the air mole flow rate at the compressor entrance increases and so is the GT net power. The GT exhaust gas mole flow rate is regulated by the air mole flow rate at the compressor entrance, and the net power consumed by the blower is affected by the GT exhaust gas mole flow rate, as shown in Figure 7B.

Figure 7C shows the comparison of $c_{CO_2}$ and $c_{O_2}$ in the GT exhaust gas and MCFC voltage of the GSCC system with SEGR in parallel and series and the reference case. For the reference system, the $c_{CO_2}$ in GT exhaust is 4.39%, which results in a low MCFC voltage as the fuel cell performance is significantly influenced by the $c_{CO_2}$ of the gas mixture fed into the MCFC cathode. With SEGR in parallel or in series, the $c_{CO_2}$ in GT exhaust gas increases, and $c_{O_2}$ is decreases, which leads to the increase in the MCFC voltage.

**TABLE 4 Parameters of the investigated configurations.**

| Parameter | Reference system | Parallel 96/90 | Series 91/28 | Series 90/36 | Series 85/46 |
|---|---|---|---|---|---|
| Recirculation rate (%) | - | 60 | - | - | - |
| MCFC $CO_2$ utilization rate | 0.85 | 0.9 | 0.28 | 0.36 | 0.46 |
| Selective $CO_2$ transfer rate | - | 0.96 | 0.91 | 0.9 | 0.85 |
| OCCR (%) | 88.16 | 88.16 | 88.16 | 88.16 | 88.16 |
| *MCFC* | | | | | |
| Voltage (V) | 0.59 | 0.725 | 0.722 | 0.721 | 0.69 |
| Current density ($A/m^2$) | 1,500 | 1,500 | 1,500 | 1,500 | 1,500 |
| Area ($m^2$) | 102,245 | 102,245 | 102,245 | 102,245 | 102,245 |
| *$CO_2$-enriched air at the compressor inlet* | | | | | |
| Temperature (K) | 298.15 | 298.15 | 298.15 | 298.15 | 298.15 |
| Pressure (MPa) | 0.102 | 0.102 | 0.102 | 0.102 | 0.102 |
| Mole flow (kmol/s) | 20.35 | 19.27 | 19.16 | 19.29 | 19.69 |
| $c_{CO_2}$ (vol%) | 0.03 | 6.6 | 7.42 | 6.6 | 4.03 |
| $c_{O_2}$ (vol%) | 20.73 | 19.1 | 17.88 | 18.28 | 19.42 |
| *Flue gas at GT exhaust* | | | | | |
| Temperature (K) | 949.03 | 970.49 | 972.48 | 969.97 | 961.91 |
| Pressure (MPa) | 0.102 | 0.102 | 0.102 | 0.102 | 0.102 |
| Mole flow (kmol/s) | 21.29 | 20.2 | 20.1 | 20.22 | 20.62 |
| $c_{CO_2}$ (vol%) | 4.39 | 10.93 | 11.72 | 10.92 | 8.38 |
| $c_{O_2}$ (vol%) | 11.29 | 8.97 | 7.75 | 8.19 | 9.48 |
| $H_2O$ concentration (vol%) | 8.79 | 9.26 | 9.3 | 9.25 | 9.07 |
| GT net power (MW) | 289.25 | 283.08 | 282.42 | 283.17 | 285.52 |
| ST net power (MW) | 157.25 | 160.05 | 160.4 | 160.03 | 158.95 |
| MCFC net power (MW) | 90.96 | 111.24 | 110.71 | 110.65 | 105.91 |
| $CO_2$ compressor (MW) | −17.77 | −17.77 | −17.77 | −17.77 | −17.77 |
| ASU (MW) | −2.24 | −2.24 | −2.24 | −2.24 | −2.24 |
| Blower (MW) | - | −3.27 | −5.77 | −5.81 | −5.95 |
| Net power output | 517.45 | 531.09 | 527.75 | 528.03 | 524.42 |
| Overall thermal efficiency (%) | 55.16 | 56.62 | 56.26 | 56.29 | 55.91 |

## 6 Economic and environmental performance evaluation

In this section, the economic and environmental performances of new systems are compared with those of the reference system.

The principal economic criteria used to assess various $CO_2$ capture methods are the specific primary energy consumption for $CO_2$ avoided (SPECCA) and the cost of $CO_2$ avoided (CCA). The equations for cost estimation are listed in Table 5. For the power section, α is 0.7, β is 0.45, and γ is 0.35; for the $CO_2$ removal section, α is 1.1, β is 0.45, and γ is 0.7 (Gatti et al., 2020).

Table 6 shows the comparison results of the economic evaluation. Contrast to the CCA of the conventional MEA technique for $CO_2$ capture (Leto et al., 2011), the overall thermal efficiency of the parallel 96/90 system in this paper is higher, which results in a negative SPECCA index. Figure 8A shows the thermodynamic performance (SPECCA) of the systems investigated. The cost per kW MCFC is fixed at 555 $/kW (Gatti et al., 2020). Over the last 20 years, the MCFC cost has been reduced significantly (Campanari et al., 2014), and further decrease exists according to DOE targets (Spendelow et al., 2012). The investment lifetime is 25 years, the fuel cost is 4.5$/GJ, and the equivalent hours at full load is 7880 h per year (Gatti et al., 2020). In Figure 8B, CCA is displayed as a function of the specific TPC ($/kW). The closer the system is to the bottom left corner, the more attractive it is because it represents lower operating and specific investment costs.

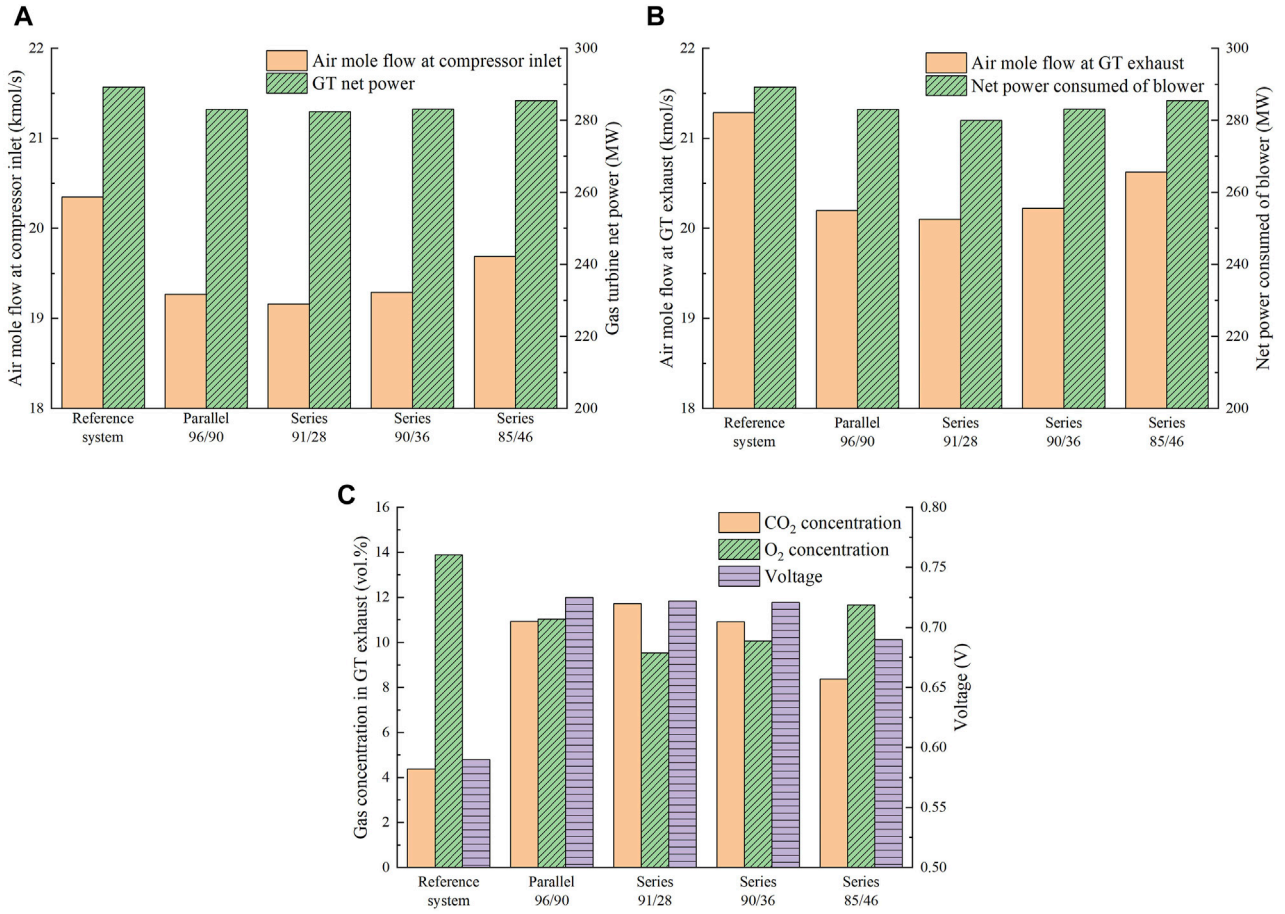


FIGURE 7
**(A)** Air mole flow at the compressor inlet and GT net power output. **(B)** GT exhaust gas mole flow and net power consumed by the blower. **(C)** $CO_2/O_2$ concentration in the GT exhaust and MCFC voltage for the GSCC system with SEGR in parallel and in series, which is in contrast to the reference system.

**TABLE 5 Equations for cost estimation.**

| | | |
|---|---|---|
| SPECCA | $SPECCA\left[\frac{MJ_{LHV}}{kg_{CO_2,avoided}}\right] = \frac{\left(\frac{1}{\eta_{CCS}}-\frac{1}{\eta_{REF}}\right)}{E_{REF}-E_{CCS}} \cdot 3600$ | (33) |
| TEC | $TEC[M\$] = C_0\left(\frac{S}{S_0}\right)^f$ | (34) |
| INST | $INST = \alpha \cdot TEC$ | (35) |
| IC | $IC = \beta \cdot (1+\alpha) \cdot TEC$ | (36) |
| EPC | $EPC = TEC + INST + IC = (1+\alpha) \cdot (1+\beta) \cdot TEC$ | (37) |
| OCC | $OCC = \gamma \cdot EPC = \gamma \cdot (1+\alpha) \cdot (1+\beta) \cdot TEC$ | (38) |
| TPC | $TPC = EPC + OCC = (1+\alpha) \cdot (1+\beta) \cdot (1+\gamma) \cdot TEC$ | (39) |
| CCA | $CCA\left[\frac{\$}{t_{CO_2}}\right] = \frac{(COE)_{CCS}-(COE)_{REF}}{(kg_{CO_2}kWh^{-1})_{REF}-(kg_{CO_2}kWh^{-1})_{CCS}}$ | (40) |

## 7 Conclusion

In this paper, the MCFC-integrated GSCC systems with $CO_2$ capture and SEGR in series/parallel are investigated and contrasted with the MCFC-integrated GSCC system with $CO_2$ capture and without SEGR (the reference case). The results show that the new systems markedly increase the $c_{CO_2}$ in the emission of the gas turbine, maintaining oxygen concentration in the combustor at above 17 vol%. The $CO_2$ concentrations of the GT exhaust gas reached 14.15 vol% and 11.72 vol% for SEGR parallel (96/90) and series (91/28), respectively, when the OCCR is 88.16%. In addition, the thermal efficiencies of new systems increasingly contrasted to that of the reference system (55.16%). For SEGR in parallel (96/90) and series (90/36), the thermal efficiencies reached 56.65% and 56.29%, respectively, which are 0.19% higher and 0.14% lower than that of the GSCC system without $CO_2$ capture (56.43%).

1) For the systems with SEGR in parallel, the OCCR is held constant at 88.16%. As the SEGR increases and the SCTR remains unchanged, the MCFC $CO_2$ utilization rate increases; when SEGR is kept unchanged and SCTR increases, the MCFC $CO_2$ utilization rate decreases. When the SEGR increases from 0.1 to 0.7 and the SCTR is held constant at 0.95, the $c_{CO_2}$ of the GT flue gas increases from 4.87% to 14.15% and the $c_{O_2}$ in the combustor inlet exhaust is reduced from 20.86% to 18.27%. When the SCTR is held constant at 0.95 and the SEGR increases from 0.1 to 0.6, the

**TABLE 6 Economic performance evaluation results of investigated systems.**

| | GSCC system without $CO_2$ capture (Duan et al., 2014) | Reference system | Parallel 96/90 | Series 90/36 |
|---|---|---|---|---|
| System fuel input ($MW_{LHV}$) | 750.6 | 938 | 938 | 938 |
| GT net power (MW) | 289.25 | 289.25 | 283.08 | 283.17 |
| ST net power (MW) | 134.34 | 157.25 | 160.05 | 160.03 |
| MCFC net power (MW) | - | 90.96 | 111.24 | 110.65 |
| $CO_2$ compressor (MW) | - | −17.77 | −17.77 | −17.77 |
| ASU (MW) | - | −2.24 | −2.24 | −2.24 |
| Blower (MW) | - | - | −3.27 | −5.81 |
| Net power (MW) | 423.59 | 517.45 | 531.09 | 528.03 |
| Overall thermal efficiency (%) | 56.43 | 55.16 | 56.62 | 56.29 |
| Specific $CO_2$ emission (g/kWh) | 349.22 | 44.34 | 43.2 | 43.45 |
| $CO_2$ avoided (%) | - | 87.3 | 87.63 | 87.56 |
| SPECCA ($MJ_{LHV}/kg_{CO_{2,avoided}}$) | - | 0.48 | −0.072 | 0.052 |
| *Plant component equipment cost* | | | | |
| Gas turbine (M$) | 62.89 | 62.89 | 62.89 | 62.89 |
| Steam turbine (M$) | 25.34 | 28.66 | 28.79 | 28.77 |
| HRSG (M$) | 28.01 | 46.08 | 41.67 | 41.66 |
| Heat rejection (M$) | 30.55 | 45.86 | 47.08 | 47.15 |
| MCFC + BOP (M$) | - | 50.48 | 61.74 | 61.41 |
| Membrane (M$) | - | - | 25.34 | 52.46 |
| ASU (M$) | - | 5.82 | 5.82 | 5.82 |
| $CO_2$ compressor (M$) | - | 16.78 | 16.78 | 16.78 |
| Power section TEC (M$) | 146.79 | 183.49 | 180.43 | 180.47 |
| Power section TPC (M$) | 488.48 | 610.61 | 600.43 | 600.56 |
| $CO_2$ removal section TEC (M$) | - | 73.08 | 109.68 | 136.47 |
| $CO_2$ removal section TPC (M$) | - | 378.3 | 567.76 | 706.44 |
| Total TPC (M$) | 488.48 | 988.91 | 1168.2 | 1307 |
| Fuel cost (M$) | 95.72 | 119.62 | 119.62 | 119.62 |
| Fixed O and M cost (M$) | 10 | 25.8 | 28 | 29.3 |
| Consumables (M$) | 6.4 | 10.22 | 12.73 | 13.3 |
| First year capital charge (M$) | 163.38 | 280.76 | 304.62 | 333.74 |
| COE ($/MWh) | 48.95 | 68.86 | 72.79 | 80.21 |
| $CO_2$ specific avoidance (g/kWh) | - | 304.88 | 306.02 | 305.77 |
| CCA ($/$t_{CO_2}$) | - | 65.3 | 77.9 | 102.23 |

system thermal efficiency increases from 55.17% to 56.64%; when the SEGR increases from 0.6 to 0.7, the system thermal efficiency decreases from 56.64% to 56.55%.

2) For the systems with SEGR in series, the OCCR is held constant at 88.16%; when the SCTR increases from 0.65 to 0.91, the MCFC $CO_2$ utilization rate is reduced from 0.66 to 0.34. When the SCTR increases from 0.65 to 0.91, the $c_{CO_2}$ of the GT flue gas increases from 5.67% to 11.72% and the $c_{O_2}$ in combustor entrance gas decreases from 20.52% to 17.88%. When the SCTR increases from 0.65 to 0.9, the system thermal efficiency increases from 55.07% to 56.29%; when the SCTR increases from 0.9 to 0.91, the system thermal efficiency is reduced from 56.29% to 56.26%.

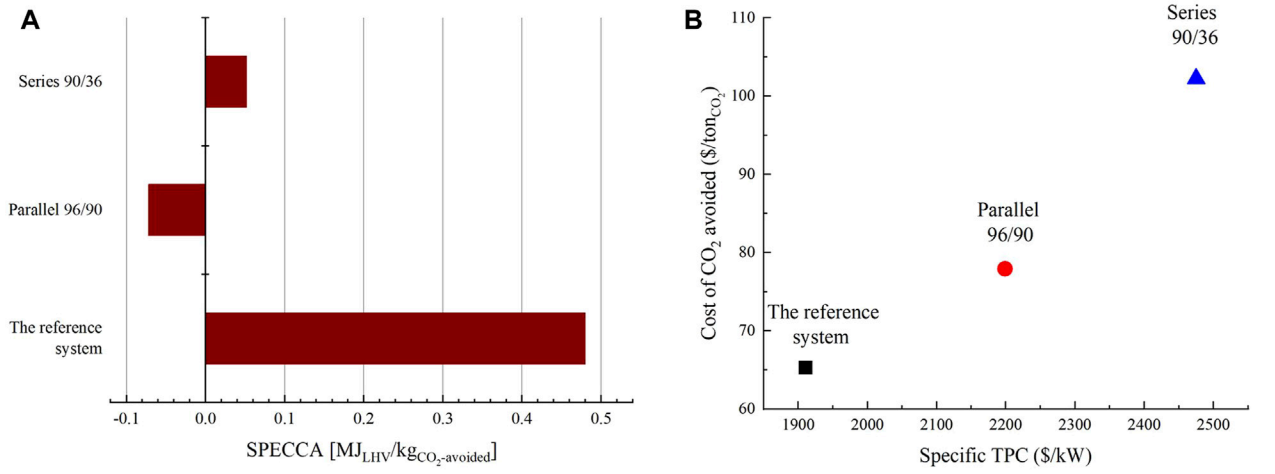


FIGURE 8
**(A)** SPECCA of the different systems and **(B)** CCA vs. specific TPC.

3) When the $CO_2$ utilization rate of the MCFC is 0.96 and the SCTR of the membrane is 0.90, the new system with SEGR in parallel exhibits a better economic and environmental performance.

Because of the high cost of the MCFC at present, the new system does not have significant advantages in terms of technical or economic performance. The advantage of the MCFC-based $CO_2$ capture system, as well as forthcoming technological improvements, will contribute to advancing its economic performance.

## Data availability statement

The original contributions presented in the study are included in the article/Supplementary Material; further inquiries can be directed to the corresponding author.

## Author contributions

JB: Conceptualization, Data curation, Investigation, Methodology, Software, Writing–original draft. LD: Project administration, Supervision, Writing–review and editing.

## Funding

The author(s) declare that financial support was received for the research, authorship, and/or publication of this article. This work was supported by the National Nature Science Foundation Project of China (No. 52076078) and the Science Fund for Creative Research Groups of the National Natural Science Foundation of China (No. 51821004).

## Conflict of interest

The authors declare that the research was conducted in the absence of any commercial or financial relationships that could be construed as a potential conflict of interest.

## Publisher's note

All claims expressed in this article are solely those of the authors and do not necessarily represent those of their affiliated organizations, or those of the publisher, the editors, and the reviewers. Any product that may be evaluated in this article, or claim that may be made by its manufacturer, is not guaranteed or endorsed by the publisher.

## Supplementary material

The Supplementary Material for this article can be found online at: https://www.frontiersin.org/articles/10.3389/fenrg.2023.1256000/full#supplementary-material

## References

Arpornwichanop, A., Saebea, D., Patcharavorachot, Y., et al. (2013). Analysis of a pressurized solid oxide fuel cell-gas turbine hybrid power system with cathode gas recirculation. *Int. J. hydrogen energy* 38, 4748–4759. doi:10.1016/j.ijhydene.2013.01.146

Bellas, J. M., Finney, K. N., Diego, M. E., Ingham, D., and Pourkashanian, M. (2019). Experimental investigation of the impacts of selective exhaust gas recirculation on a micro gas turbine. *Int. J. Greenh. Gas Control* 90, 102809. doi:10.1016/j.ijggc.2019.102809

Bian, J., Duan, L., Lei, J., and Yang, Y. (2020). Study on the entropy generation distribution characteristics of molten carbonate fuel cell system under different $CO_2$ enrichment conditions. *Energies* 13, 5778. doi:10.3390/en13215778

Bian, J., Zhang, H., Duan, L., Desideri, U., and Yang, Y. (2022). Study of an integrated gas turbine -Molten carbonate fuel cell -organic Rankine cycle system with $CO_2$ recovery. *Appl. Energy* 323, 119620. doi:10.1016/j.apenergy.2022.119620

Campanari, S., Chiesa, P., Manzolini, G., and Bedogni, S. (2014). Economic analysis of $CO_2$ capture from natural gas combined cycles using molten carbonate fuel cells. *Appl. Energy* 130, 562–573. doi:10.1016/j.apenergy.2014.04.011

Carapellucci, R., Battista, D. D., and Cipollone, R. (2019). The retrofitting of a coal-fired subcritical steam power plant for carbon dioxide capture: a comparison between MCFC-based active systems and conventional MEA. *Energy Convers. Manag.* 194, 124–139. doi:10.1016/j.enconman.2019.04.077

Choi, J. H., Ahn, J. H., and Kim, T. S. (2014). Performance of a triple power generation cycle combining gas/steam turbine combined cycle and solid oxide fuel cell and the influence of carbon capture. *Appl. Therm. Eng.* 71 (1), 301–309. doi:10.1016/j.applthermaleng.2014.07.001

Diego, M. E., Bellas, J. M., Mohamed, P., et al. (2018). Techno-economic analysis of a hybrid CO2 capture system for natural gas combined cycles with selective exhaust gas recirculation. *Appl. Energy* 215, 778–791. doi:10.1016/j.apenergy.2018.02.066

Duan, L., Sun, S., Yue, L., Qu, W., and Yang, Y. (2015). Study on a new IGCC (integrated gasification combined cycle) system with $CO_2$ capture by integrating MCFC (molten carbonate fuel cell). *Energy* 87, 490–503. doi:10.1016/j.energy.2015.05.011

Duan, L., Zhu, J., Long, Y., and Yang, Y. (2014). Study on a gas-steam combined cycle system with $CO_2$ capture by integrating molten carbonate fuel cell. *Energy* 74, 417–427. doi:10.1016/j.energy.2014.07.006

ElKady, A. M., Evulet, A., Brand, A., Ursin, T. P., and Lynghjem, A. (2009). Application of exhaust gas recirculation in a DLN F-class combustion system for postcombustion carbon capture. *J.Eng. Gas. Turbines Power* 131 (5), 34505. doi:10.1115/1.2982158

Evulet, A. T., Elkady, A. M., Branda, A. R., and Chinn, D. (2009). On the performance and operability of GE's dry low NO combustors utilizing exhaust gas recirculation for PostCombustion carbon capture. *Energy Procedia* 1, 3809–3816. doi:10.1016/j.egypro.2009.02.182

Franz, J., Schiebahn, S., Zhao, L., Riensche, E., Scherer, V., and Stolten, D. (2013). Investigating the influence of sweep gas on $CO_2/N_2$ membranes for post-combustion capture. *Int. J. Greenh. Gas Control* 13, 180–190. doi:10.1016/j.ijggc.2012.12.008

Gatti, M., Martelli, E., Di Bona, D., Gabba, M., Scaccabarozzi, R., Spinelli, M., et al. (2020). Preliminary performance and cost evaluation of four alternative technologies for post-combustion CO2 capture in natural gas-fired power plants. *Energies* 13, 543. doi:10.3390/en13030543

Hayre, R. (2006). *Fuel cell fundamentals*. Hoboken, New Jersey, United States: Wiley.

Herraiz, L., Fernández, E. S., Palfi, E., and Lucquiaud, M. (2018). Selective exhaust gas recirculation in combined cycle gas turbine power plants with post-combustion $CO_2$ capture. *Int. J. Greenh. Gas Control* 71, 303–321. doi:10.1016/j.ijggc.2018.01.017

Leto, L., Dispenza, C., Moreno, A., and Calabro, A. (2011). Simulation model of a molten carbonate fuel cell–microturbine hybrid system. *Appl. Therm. Eng.* 31 (6-7), 1263–1271. doi:10.1016/j.applthermaleng.2010.12.029

Merkel, T. C., Zhou, M., and Ba Ker, R. W. (2012). Carbon dioxide capture with membranes at an IGCC power plant. *J. Membr. Sci.* 389, 441–450. doi:10.1016/j.memsci.2011.11.012

Miao, L., Tang, S., Li, X., Yu, D., Deng, Y., Hang, T., et al. (2022). Estimating the CO2 emissions of Chinese cities from 2011 to 2020 based on SPNN-GNNWR. *Environ. Res.* 218, 115060. doi:10.1016/j.envres.2022.115060

Milewski, J., Bujalski, W., Woowicz, M., Futyma, K., and Bernat, R. (2013). Experimental investigation of $CO_2$ separation from lignite flue gases by 100 $cm^2$ single molten carbonate fuel cell. *Appl. Mech. Mater.* 376 (3), 299–303. doi:10.4028/www.scientific.net/AMM.376.299

Ramasubramanian, K., Verweij, H., and Ho, W. S. W. (2012). Membrane processes for carbon capture from coal-fired power plant flue gas: a modeling and cost study. *J. Membr. Sci.* 2012, 299–310. doi:10.1016/j.memsci.2012.07.029

Richard, W., Baker, Kniep, J., Wei, X., and Merkel, T. (2017). $CO_2$ capture from natural gas power plants using selective exhaust gas recycle membrane designs. *Int. J. Greenh. Gas Control* 66, 35–47. doi:10.1016/j.ijggc.2017.08.016

Spendelow, J., Nguyen, T., Houchins, C., et al. (2012). Medium-scale CHP fuel cell system targets. https://www.hydrogen.energy.gov/pdfs/11014_medium_scale_chp_target.pdf (accessed on April 27, 2023).

Tsukagoshi, K., Muyama, A., Masada, J., et al. (2007). Operating status of uprating gas turbines and future trend of gas turbine development. *Tech. Rev. - Mitsubishi Heavy Ind.* 44 (4).

Zhao, H., and Hou, Q. (2022). Study on thermal performance of solar methanol reforming MCFC-GT-ST-CHP system. *Hydrogen Energy* 47, 28670–28683. doi:10.1016/j.ijhydene.2022.06.195

# Nomenclature

| | |
|---|---|
| **A** | area, $m^2$ |
| $A_c$ | cell active area, $m^2$ |
| **ASU** | air separation unit |
| **BOP** | balance of the plant |
| $c_{CO_2}$ | $CO_2$ concentration |
| $c_{O_2}$ | $O_2$ concentration |
| **CCA** | cost of $CO_2$ avoided, $/ton$_{CO_2}$ |
| **COE** | cost of electricity, $/MWh |
| $D_{eff}$ | effective diffusivity, $m^2/s$ |
| **ECO$_2$** | $CO_2$-specific emissions, g/kWh |
| $E_{Nerst}$ | ideal reversible voltage, V |
| **EPC** | engineering, procurement, and construction costs, M$ |
| **F** | Faraday constant, 96,487 C/mol |
| $\Delta G$ | Gibbs free energy, kJ/kg |
| **GSCC** | gas–steam combined cycle |
| **GT** | gas turbine |
| **HRSG** | heat recovery steam generator |
| **IC** | indirect cost, M$ |
| **IDC** | interest during construction, M$ |
| **IGCC** | integrated gasification combined cycle |
| **INST** | installation cost, M$ |
| **J** | current density, $A/m^2$ |
| $j_0$ | exchange current density, $A/m^2$ |
| $j_0^0$ | standard exchange current density, $A/m^2$ |
| $LHV$ | low heat value of fuel, kJ/kg |
| $m_{CO_2,inlet}$ | $CO_2$ mass flow rate in the cathode inlet, kg/s |
| $m_{CO_2,outlet}$ | $CO_2$ mass flow rate in the cathode outlet, kg/s |
| $m_{fuel,inlet}$ | fuel mass flow rate in the anode inlet, kg/s |
| $m_{fuel,outlet}$ | fuel mass flow rate in the anode outlet, kg/s |
| $m_{MCFC}^{\cdot}$ | mass flow rate of MCFC input fuel, kg/s |
| $m_{GT}^{\cdot}$ | mass flow rate of gas turbine input fuel, kg/s |
| **MCFC** | molten carbonate fuel cell |
| **N** | number of single cells |
| **NGCC** | natural gas combined cycle |
| $n$ | number of electrons released in the dissociation of $H_2$ molecule |
| **OCC** | owner's cost and contingencies |
| **SPECCA** | specific primary energy consumption per unit of $CO_2$ avoided |
| **SPP** | steam power plant |
| **TEC** | total equipment cost |
| **TPC** | total plant cost |
| $\eta_{DC-AC}$ | conversion efficiency of DC (direct current) into AC (alternative current) |
| $\eta_{ohm}$ | Ohmic voltage loss, V |
| $\eta_{conc}$ | concentration voltage loss, V |
| $\tau$ | thickness, mm |
| $\sigma$ | electrical conductivity, $S/m^{-1}$ |

**Subscripts**

| | |
|---|---|
| **act** | activation |
| **an** | anode |
| **ca** | cathode |
| **conc** | concentration |
| **elec** | electrolyte |
| **f** | feed side |
| **i** | species i |
| **ohm** | Ohmic |
| **p** | permeate side |
| **TPB** | three-phase boundary |